frontiers in Energy Research

REVIEW
published: 27 March 2019
doi: 10.3389/fenrg.2019.00028

Roles of Ti in Electrode Materials for Sodium-Ion Batteries

*Yuesheng Wang, Wen Zhu, Abdelbast Guerfi, Chisu Kim and Karim Zaghib**

Center of Excellence in Transportation Electrification and Energy Storage, Hydro-Québec, Varennes, QC, Canada

Sodium-ion batteries offer a promising alternative to lithium-ion batteries due to their low cost, environmental friendliness, high abundance of sodium, and established electrochemical process. However, problems, such as low capacity, low storage voltage and capacity fade of electrode materials, must be resolved for the applications of sodium ion batteries. Many Ti-containing compounds were reported as cathode and anode materials, but very few studies focus on the role of Ti in electrodes used in sodium-ion batteries. This paper systemically reviews the roles of Ti in electrodes of sodium ion batteries. The Ti^{4+}/Ti^{3+} redox couple is a good choice for anodes due to its low potential and it exhibits different storage voltages in different structures. Although Ti^{4+} does not participate in charge transfer in cathodes, it can indirectly enhance the capacity, cycling life and rate performance via structure change, cation order-disorder transition, and its interaction with the crystal lattice structure. This review will provide a new insight in designing and understanding novel high-performance electrodes.

Keywords: sodium ion batteries, cathode, anode, titanium–based composite, order—disorder phase transition

OPEN ACCESS

Edited by:
Renaud Bouchet,
Université Grenoble Alpes, France

Reviewed by:
Kai Zhu,
Harbin Engineering University, China
Wenping Sun,
University of Wollongong, Australia

****Correspondence:***
Karim Zaghib
zaghib.karim@ireq.ca

Specialty section:
This article was submitted to Electrochemical Energy Conversion and Storage, a section of the journal Frontiers in Energy Research

Received: *17 December 2018*
Accepted: *05 March 2019*
Published: *27 March 2019*

Citation:
Wang Y, Zhu W, Guerfi A, Kim C and Zaghib K (2019) Roles of Ti in Electrode Materials for Sodium-Ion Batteries. Front. Energy Res. 7:28. doi: 10.3389/fenrg.2019.00028

INTRODUCTION

Due to environmental concerns associated with gasoline engines, electric vehicles (EVs) powered by lithium-ion batteries are becoming increasingly popular (Armand and Tarascon, 2008). However, the high cost and safety issues of lithium-ion batteries (LIB) are limiting their practical applications (Goodenough and Kim, 2009) and provide an opportunity for other batteries to meet the needs of energy storage (Dunn et al., 2011; Yang et al., 2011; Wang et al., 2018a). Sodium-ion batteries (SIB) have the advantage of an abundant sodium resource and compatibility with an aluminum current collector for both cathodes and anodes, which reduce battery cost and make them a promising alternative to lithium ion batteries (Pan et al., 2013a; Slater et al., 2013).

Research on sodium-ion batteries began in the early 1980's (Delmas et al., 1980), but the successful commercialization of lithium ion batteries in 1990 distracted the attention from research and development of SIB (Ellis and Nazar, 2012). Since 2010, numerous novel electrode materials for sodium-ion batteries have been reported. The cathodes are classified according to their structure, namely, Prussian blue, NASICON, olivine, tunnel-type, and oxides. Prussian blue analogs are attractive cathodes for sodium-ion batteries due to their open channel-like structure, compositional and electrochemical tenability. But water control during synthesis and the potential toxicity from cyanide release limit their applications (Wessells et al., 2011a,b). NASICON compounds, such as $Na_3V_2(PO_4)_3$ and $Na_3V_2(PO_4)_2F_3$, were also used as electrodes for sodium-ion batteries. $Na_3V_2(PO_4)_3$/C cathode has a voltage plateau of 3.4 V with capacity of ~100 mAh/g, excellent rate capacity and cycle stability (Jian et al., 2012), whereas $Na_3V_2(PO_4)_2F_3$ compounds possess two plateaus at 3.6 and 4.1 V as well as a capacity of 100 mAh/g in the 2.5–4.3 V voltage range. Although these cathodes exhibit promising Na storage performance, the highly toxic V^{3+}/V^{5+} and the

possibility of releasing fluorine gas becomes an environmental issue in large-scale production (Gover et al., 2006). Unlike $LiFePO_4$, the olivine $NaFePO_4$ is thermally unstable in ambient environment and has to be produced (Kim et al., 2015) by the ion exchange of Li^+ in olivine $LiFePO_4$ with Na^+, which complicates the production and increases cost (Oh et al., 2012). The commercial success of layered-$LiCoO_2$ in lithium-ion batteries (Mizushima et al., 1980) has prompted extensive investigation of its sodium counterpart Na_xTMO_2 (TM: Ni, Mn, Co, Ti) which crystallize into layered or tunneled structures depending on sodium content. The layered-structure consists of TM-O and Na-O layers. Compared to Li^+, Na^+ has a larger radius and stronger interaction with O^{2-}. The sodium-layered structure is further divided into O3, P3, P2, and O2. The O and P represent the octahedral and trigonal prismatic coordination environment of alkali ions, respectively; 3 and 2 describe the number of TM layers of repeated stacking (Delmas et al., 1980). The oxides P2/O3-Na_xCoO_2, Na_xMnO_2 Na_xVO_2 and Na_xNiMnO_2 etc. are also investigated (Delmas et al., 1981; Braconnier et al., 1982; Maazaz et al., 1983; Miyazaki et al., 1983; Jeong and Manthiram, 2001; Lu and Dahn, 2001), and some of the plateaus in the charge/discharge profile are attributed to Na^+/vacancy ordering, which affects the rate and cycling performance. Electrodes-containing Ti, such as $Na_{0.6}Cr_{0.6}Ti_{0.4}O_2$, $Na_{2/3}Ni_{1/3}Mn_{1/2}Ti_{1/6}O2$, $Na_{0.8}Ni_{0.4}Ti_{0.6}O_2$, and $Na_{0.67}Co_{0.33}Ti_{0.67}O_2$, etc., show a smooth sloping curve during sodium insertion and extraction, suggesting that Ti-substitution interrupted the Na^+/vacancy ordering (Yoshida et al., 2014; Yu et al., 2014; Guo et al., 2015a; Wang et al., 2015c). Tunnel-type $Na_{0.44}MnO_2$ was first proposed as a cathode by Doeff et al. (1994). It has a unique structure that prevents interaction with H_3O^+, which is useful as a cathode or anode for non-aqueous and aqueous sodium-ion batteries (Whitacre et al., 2010; Hosono et al., 2012). Ti- substitution for Mn in $Na_{0.44}MnO_2$ smooth's its multi-plateaus discharge-charge curve (Wang et al., 2015a).

The carbon-based compounds (Alcántara et al., 2001; Li et al., 2015, 2016b; Zheng et al., 2017; Wang et al., 2018b), alloys (Xiao et al., 2012; Farbod et al., 2014; Lim et al., 2017), organic compounds (Wang et al., 2014; Wu et al., 2015d), sulfides (Newman and Klemann, 1980), phosphates (Wu et al., 2013; Pang et al., 2014), and oxides (Senguttuvan et al., 2011; Trinh et al., 2012; Pan et al., 2013b; Sun et al., 2013; Wang et al., 2013; Xu et al., 2014; Zhao et al., 2015; Ding et al., 2017) are widely investigated as anodes. Hard carbon, obtained at high temperatures (1,600°C), exhibits a high reversible capacity of 330 mAh/g at a rate of 0.1C in the range of 0–2.5 V (Lu et al., 2018; Wang et al., 2018b; Zhao et al., 2018b). The near zero voltage vs. Na^+/Na may result in sodium metal deposition on a hard carbon surface caused by improper battery operation or fast charging, which is a major safety concern (Chevrier and Ceder, 2011). In addition, low initial columbic efficiency and relatively high cost need to be resolved for practical application (Zhang et al., 2016). Although alloys, such as Sb/C (610 mAh/g) (Darwiche et al., 2012; Wu et al., 2014), SnSb/C (544 mAh/g) (Xiao et al., 2012), P (1,800 mAh/g) (Ramireddy et al., 2015), deliver high reversible capacities, the large volume change during cycling leads to electrode instability, a common problem in lithium-ion batteries too (Goodenough and Kim, 2009; Chevrier and Ceder, 2011). Organic compounds, such as $Na_2C_8H_4O_4$, $Na_2C_{16}H_{10}O_4$ etc., are also actively explored for sodium-ion batteries due to their low cost and high performance (Zhao et al., 2012b; Wang et al., 2014; Wu et al., 2015d). But the poor electronic conductivity, low initial coulombic efficiency, and poor cyclic stability still need to be improved. Sulfide electrodes, for example, TiS_2 and MoS_2, with ∼200 $mAhg^{-1}$ at the storage voltage of 2.0 V, have been investigated since 1976, but the voltage is slightly higher for the anode and the samples are sensitive to air (Silbernagel and Whittingham, 1976; Newman and Klemann, 1980; Hu et al., 2014). NASICON-type $NaTi_2(PO_4)_3$, obtained by Ti^{4+}/Ti^{3+} conversion, exhibits a reversible Na storage capacity of ca. 120 mAh/g at 2.1 V vs. Na^+/Na, which is suitable as an anode for aqueous sodium-ion batteries (Park et al., 2011; Li et al., 2013; Wang et al., 2015b). Metal-oxides, e.g., Fe_2O_3, Sb_2O_4 and MnO_2 etc. demonstrate a capacity around 200 mAh/g; however, the conversion reaction involved in charge transfer may result in low initial coulombic efficiency and electrode instability (Reddy and Reddy, 2004; Sun et al., 2011; Jian et al., 2014). Ti-containing oxides, such as $Li_4Ti_5O_{12}$, attracted a lot of attention due to their high reversibility in lithium-ion batteries (Ferg et al., 1994; Wagemaker et al., 2008). Research on Ti-containing oxides has expanded since 2010. For example, monoclinic $Na_2Ti_3O_7$ (Senguttuvan et al., 2011); spinel $Li_4Ti_5O_{12}$ (Zhao et al., 2012a), P2-layered $Na_{0.66}Li_{0.22}Ti_{0.78}O_2$ (Wang et al., 2013), O3-type $Na_{0.68}Mg_{0.34}Ti_{0.66}O_2$ (Zhao et al., 2018a), Anatase/Rutile TiO_2 (Wu et al., 2015b; Lan et al., 2017), $NaTiOPO_4$ (Mu et al., 2016) and $NaTiO_2$ (Wu et al., 2015a). All of these oxides exhibit Ti^{3+}/Ti^{4+} charge transfer, but the sodium storage voltages are very different.

Herein, we focused on the roles of Ti in electrodes for sodium-ion batteries. Various Ti-containing compounds are shown in **Figure 1**. In anode materials, Ti^{4+}/Ti^{3+} participate in charge transfer and demonstrate different electrochemical performances corresponding to their different structures. In the cathode, the doped Ti^{4+} in Na_xTMO_2 oxides does not participate in charge transfer. However, Ti-substitution results in a structural change that interrupts the Na^+/vacancy orderings, which in turn affects the capacity, cycling and rate performance. This review provides a deep understanding of the Ti's roles in the development of novel materials for sodium-ion batteries.

Anode Materials

Titanium dioxides with different polymorphs, such as anatase, rutile, TiO_2 (B) and amorphous, have been explored as anode materials for sodium ion batteries due to their high theoretical capacity of 335 mAh/g, high rate performance, good cyclability, non-toxicity and low cost (Xiong et al., 2011; Wu et al., 2015b; Lan et al., 2017; Li et al., 2017; He et al., 2018). In addition, Density Function Theory (DFT) calculations show that the energy required for insertion of two Na^+ into unit cells of anatase and rutile are 11.10 and 20.65 eV, respectively. The difference in the energy values indicate an easier and faster Na^+ intercalation as well as diffusion in anatase than in rutile, which is due to the presence of 2D tunnels in the anatase structure (Su et al., 2015).

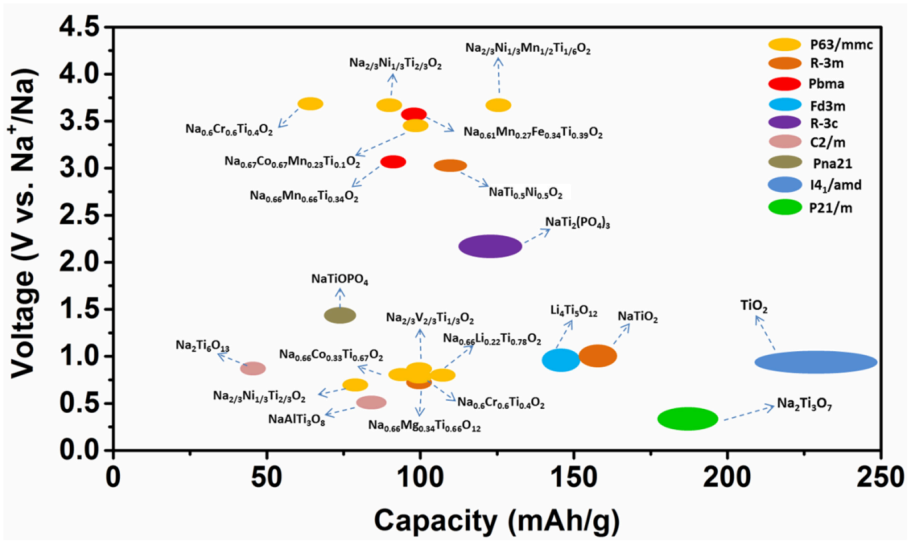

FIGURE 1 | A comparison of Ti-based electrode materials in sodium-ion batteries.

As such, the electrochemical performance of anatase is better than rutile. On the other hand, DFT calculations predict that introduction of defects in the structure can narrow the energy gap in rutile, increase the electronic conductivity and Na^+ diffusivity , as well as the rate performance, which are proved by experimental results (Chen et al., 2015; Usui et al., 2015; He et al., 2017).

TiO_2

Anatase

Anatase TiO_2 has tetragonal unit cell with space group (S.G.) I41/amd. Its crystal structure is built on corner and edge sharing of TiO_6 octahedra. There are two dimensional tunnels along its *a* and *b* axes, which facilitate Na^+ diffusion and accommodation. Despite the reduction of titanium ion to metal (Ti^0) detected on the electrode surfaces, it is attributed to the side reactions at the electrolyte/electrode interface, whereas the $Ti^{4+} \leftrightarrow Ti^{3+}$ redox reaction is considered as the contribution to the reversible capacity of the electrode. Although different shapes of sodium discharge/charge curves (with no obvious potential plateaus and with mulita-plateaus) are reported, the investigations on the reaction mechanism suggest that the capacity observed at the high potential section ($> \sim 0.8$ V) during discharge is mainly associated to the pseudo-capacitive process as well as the side reactions and SEI layer formation. Further discharge to 0.01/0.1 V, the crystallinity of anatase decreases greatly due to the insertion of Na^+ in the octahedral sites in the crystal structure. This crystallinity to amorphous/partial amorphous transition is irreversible upon the extraction of Na ions during charge (Wu et al., 2015b; Li et al., 2017). In fact, certain amounts of Na ions still rest in the host crystal structure after charge, the estimated reversible Na^+ insertion/extraction is ~ 0.41 Na^+ per TiO_2 ($V_{cut\ off\ discharge} = 0.1$ V) corresponding to ~ 140 mAh/g (Wu et al., 2015c). On the other hand, the preservation of anatase's crystallinity during Na^+ insertion is also reported, even to a low voltage of 0.01 V (Kim et al., 2014) and 0 V (González et al., 2014). In spite of the discrepancies concerning the crystallinity of anatase during cycling, the working mechanism of the electrode is agreed to be the redox reaction between Ti^{4+} and Ti^{3+} introduced by Na^+ insertion/extraction, see **Figure 2A**.

Rutile

The rutile TiO_2 crystal has a tetragonal unit cell with S.G. P42/mnm, with the Ti^{4+} ions surrounded by an octahedron of 6 oxygen atoms. The TiO_6 octahedrons are connected with edge and corner sharing. The rutile structure has a one-dimensional tunnel that enables the Na^+ to diffuse through and accommodates them, making rutile a candidate anode material for Na-ion batteries. Despite this, rutile has good cycling stability and high sodium storage performance, and it is rarely studied compared to its counterpart, anatase, due to slow sodium diffusion (Usui et al., 2015) and its very low electronic conductivity (Chen et al., 2015). Substitution of Ti^{4+} with non-tetravalent cations is considered an effective way to enhance Na^+ diffusivity and electric conductivity owing to the increased amount of vacancies. In fact, the measured electronic conductivities of doped rutile are 3–4 orders higher than the un-doped one, which agrees to the decreased band gap energy predicated by DFT calculation and leads to the high rate performance. The Fe and Nb doped rutile anodes were investigated and they showed high capacity (Fe-TiO_2, 327.1 mAh/g at 16.8 mA/g) and high rate performance (Nb-TiO_2, 120 mAh/g at 16.75A/g) (Usui et al., 2015; He et al., 2017). Their galvanostatic discharge-charge profiles show rounded potential shoulders below 1 V which are attributed to the Ti^{4+}/Ti^{3+} redox reaction due to reversible Na^+ insertion and extraction in the rutile structure, whereas the part above is assigned to the pseudo-capacitive sodium ion adsorption as well as the side reactions and SEI formation. XRD analysis demonstrated that (1) crystal

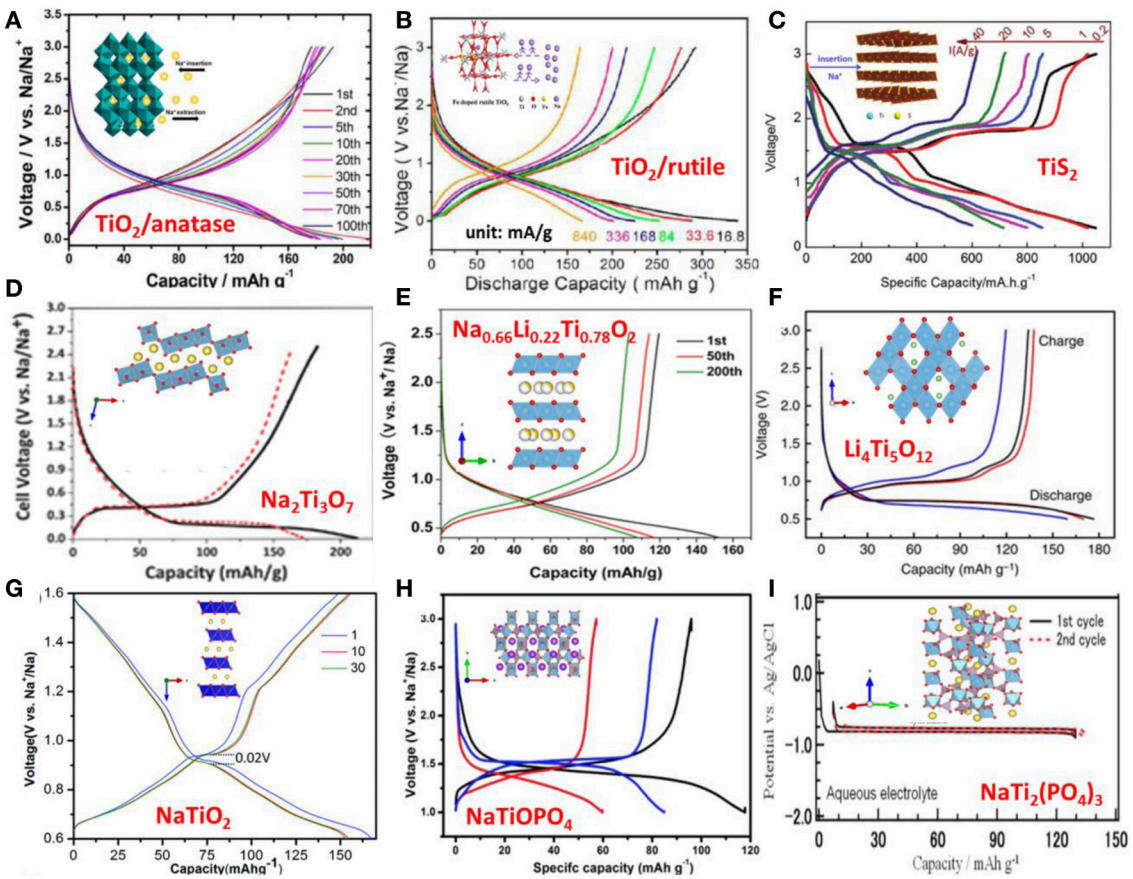

FIGURE 2 | The structure and charge–discharge profiles of **(A)** Anatase TiO_2, with permission from ACS; **(B)** Rutile TiO_2, with permission from ACS; **(C)** TiS_2, With permission from Wiley; **(D)** $Na_2Ti_3O_7$; with permission from RSC. **(E)** $Na_{0.66}Li_{0.22}Ti_{0.78}O_2$; with permission from Springer. **(F)** $Li_4Ti_5O_{12}$; with permission from Springer. **(G)** $NaTiO_2$; with permission from ACS. **(H)** $NaTiOPO_4$; with permission from RSC. **(I)** $NaTi_2(PO_4)_3$. With permission from ECS.

structure change of rutile is reversible and its crystallinity is maintained during cycling; Na ions rest in the octahedral sites, formed by corner-sharing of the octahedrons, during discharge leading to the lattice expansion in *a* axis direction; whereas *a* axis contraction is observed during charge; (2) no Na_2O and Ti metal are observed during discharge. Based on the analysis, the working mechanism of rutile is considered not based on conversion reaction, but based on intercalation/de-intercalation of Na^+, similar to the case of anatase, **Figure 2B**.

TiS_2

TiS_2 has been investigated as an anode material for sodium ion battery for similar reasons as TiO_2. Four electrons can be transferred through electrochemical conversion of TiS_2 to metallic Ti, leading to a theoretical capacity of 957 mA h/g (Tao et al., 2018).

TiS_2 has a layered structure with a van der Waals force bounding the TiS_2 layers. Every layer contains two hexagonally closed packed S atoms sublayers with Ti^{4+} sandwiched in between. Ti^{4+} is located at the center of S octahedron and each sulfide is connected to three Ti^{4+} ions. TiS_2 crystallizes into a hexagonal lattice with space group $P\bar{3}m1$. As an anode material of sodium ion battery; the weak van der Waals force between TiS_2 layers facilitates the Na^+ intercalation/de-intercalation and diffusion during discharge/charge. The working mechanism of TiS_2 electrode has been studied in the voltage window of 0.3 to 3 V. The phase transformation is proposed as a reversible stepwise intercalation followed by a conversion reaction:

$$TiS_2 + Na^+ + e \leftrightarrow NaTiS_2 + Na^+ + e \leftrightarrow Ti_{0.77}S + Na_2S \quad \text{initial cycle}$$

$$TiS_2 + Na^+ + e \leftrightarrow NaTiS_2 + Na^+ + e \leftrightarrow Ti_{0.77}S + Ti_{metal} + Na_2S \quad \text{subsequent cycles}$$

Some intermediate compounds also appeared before forming $NaTiS_2$, such as $Na_{0.22}TiS_2$ and $Na_{0.55}TiS_2$. Obviously, after activation of the electrode material in the initial cycle, Ti^{4+} was reduced to a lower valence state (Ti^0) in the subsequent cycles, whereas conversion of $NaTiS_2$ to Ti_{metal} and Na_2S was not seen with the cut off voltage of 1 V (Liu et al., 2016). DFT calculations proposed that TiS_2 is a semi-conductor in nature whereas $NaTiS_2$ and $Ti_{0.77}S$ are more metallic, which can enhance the electronic

conductivity of the electrode, leading to the excellent rate capacity of 621 mAh/g at 40 A/g (Tao et al., 2018), **Figure 2C**.

Spinel-$Li_4Ti_5O_{12}$

The spinel $Li_4Ti_5O_{12}$, a well-known "zero-strain" anode material for long-life lithium-ion batteries (Ferg et al., 1994; Chen et al., 2001; Wagemaker et al., 2008), is considered a promising anode for sodium ion batteries. The spinel $Li_4Ti_5O_{12}$ follows a typical bi-phase reaction mechanism and exhibits a flat voltage plateau of 1.55 V vs. Li^+/Li and high rate performance in lithium-ion batteries.

Hu et al. first investigated $Li_4Ti_5O_{12}$ as anode material for sodium-ion batteries in 2013 (Sun et al., 2013). The spinel-$Li_4Ti_5O_{12}$ (shown in **Figure 2F**) has a cubic lattice; its symmetry is described by Fd-3m space group with eight formula units of $(Li)^{8a}[Li_{1/3}Ti_{5/3}]^{16d}(O_4)^{32e}$. Each unit cell consists of three sub-lattices sites, 8a, 16d, and 32e. The Li and O ions completely occupy the tetrahedral 8a sites and the octahedral 32e sites, respectively, while the octahedral 16d sites are randomly occupied by Li and Ti ions at the ratio of 1:5. During Li intercalation, the Li^+ ions originally reside on the 8a sites, together with the newly incorporated Li^+ ions, fill the 16c sites (Samin et al., 2015). In sodium-ion batteries, $Li_4Ti_5O_{12}$ exhibits a stable specific capacity of 155 mAh/g with coulombic efficiency of >99% at a sodium storage voltages of 0.93 V and current rate of 0.1C. This storage voltage is higher than the sodium metal deposition voltage, making it safer than hard carbon. Hu et al. combined density DFT calculations, *in-situ* synchrotron XRD and scanning transmission electron microscope (STEM) imaging techniques to predict and confirm the three-phase separation mechanism, which was different from the bi-phase reaction mechanism in lithium-ion batteries. Upon discharge, Na^+ ions will occupy the 16*c* sites exclusively to form a Na_6Li phase, and at the same time, Li^{8a} ions are pushed to the nearest neighbor $Li_4Ti_5O_{12}$ (Li_4) phase to form $Li_7Ti_5O_{12}$ (Li_7) phase which is equivalent to a lithium insertion process. In this manner two new phases, Na_6Li and Li_7, are created. As discharge continues without further nucleation of Na_6Li, sodium insertion will proceed on the Na_6Li/Li_7 boundary, resulting in the transformation of Li to a Na_6Li phase and pushing this boundary forward. Meanwhile, the Li^{16c} ions from the initial Li_7 phase will diffuse into the nearby Li_4 phase to form Li_7 and thus the Li_7/Li_4 boundary proceeds. Although the operating voltage and high capacity are attractive, three-phase separation causes electrode cracking and delaminating from the current collector, adversely affecting cycle life. Furthermore, a full battery cell with the spinel-$Li_4Ti_5O_{12}$ as an anode and $Na_3V_2(PO4)_3$/C as a cathode has been tested. It displays an average operating voltage plateau at ∼2.4 V and delivers 135 mAh/g based on mass of anode. The electrochemical performance can be further enhanced by optimizing both electrodes and their weight ratio (Sun et al., 2013).

P2-Type Layered Oxides

Hu et al. explored a new "zero-strain" anode $Na_{0.66}[Li_{0.22}Ti_{0.78}]O_2$ (as shown in **Figure 2E**) with a P2-layered structure, which is an analog to $Li_4Ti_5O_{12}$, as a promising electrode material for room-temperature sodium-ion batteries (Wang et al., 2013). In this structure, the large sodium ions occupy the trigonal prismatic sites in one layer, whereas smaller Li and Ti ions co-occupy the neighboring layer. In addition, some of the Na ions (0.425) occupy the 2d site sharing the edges with the TiO_6 octahedra, whereas others (0.211) occupy the 2b site sharing two faces with the TiO_6 octahedra. This situation is similar to other P2 materials. The reversible capacity of $Na_{0.66}[Li_{0.22}Ti_{0.78}]O_2$ is ca. 110 mAh/g, and the average sodium storage voltage is ca. 0.75 V. The volume change during sodium insertion and extraction was only 0.77%, indicative of "zero-strain" characteristics; the material exhibits over 1,200 cycles with a capacity retention of 75%. The measured Na^+ ion diffusion coefficient is ca. 1×10^{-10} cm^2/s. It is also interesting to find out that the final discharge product is a mixture of several phases that retained the P2-structure, as confirmed by *in-situ* and *ex-situ* X-ray diffraction (XRD). The differences in these P2-phases lie in the sodium compositions and occupations (2b, 2d). These results demonstrate that P2-layered oxides are promising anode materials for long-life rechargeable sodium-ion batteries. In addition, P2-layered $Na_{0.6}Cr_{0.6}Ti_{0.4}O_2$ (Wang et al., 2015c), P2-$Na_{0.66}Co_{0.33}Ti_{0.67}O_2$ (Guo et al., 2015b), $Na_{0.67}Ni_{0.33}Ti_{0.67}O_2$ (Shanmugam and Lai, 2014), and $Na_{2/3}V_{2/3}Ti_{1/3}O_2$ (Fielden et al., 2017) showed similar sodium storage voltage around 0.75 V and capacity ca. 100 mAh/g with low volume change during sodium intercalation/extraction.

In some P2 layered oxides, such as $Na_{0.6}Cr_{0.6}Ti_{0.4}O_2$, $Na_{0.67}Ni_{0.33}Ti_{0.67}O_2$ and $Na_{2/3}V_{2/3}Ti_{1/3}O_2$, the valence states of Cr/Ni/V are $3^+/2^+/3^+$, which can be oxidized to $4^+/3^+/4^+$ on Na de-intercalation, enabling them as possible positive electrodes. Additionally, the valence state of Ti in these compounds is 4^+; it can be reduced to 3^+ on Na intercalation, making it a possible negative electrode. On the basis of these results, a sodium-ion full cell has been demonstrated using the same material as both negative and positive electrodes, for example, P2-$Na_{0.6}[Cr_{0.6}Ti_{0.4}]O_2$. The greatest advantage of using the same materials as both negative and positive electrodes is reducing the process cost of electrodes significantly. The symmetric full cell using P2-$Na_{0.6}[Cr_{0.6}Ti_{0.4}]O_2$ delivers an average operating voltage plateau at ∼2.53 V. The energy densities of this system are calculated to be 82 and 94 Wh/kg at current rates of 1C and C/5 based on the mass of positive and negative electrodes.

O3-Layered Oxides

In 1983, $NaTiO_2$ was first investigated as an electrode for sodium ion batteries by Maazaz et al. (1983). $NaTiO_2$ (shown in **Figure 2G**) adopts the α-$NaFeO_2$, structure which is an ordered variant of the rock-salt structure. The layers of edge-sharing TiO_6 octahedra and edge-sharing NaO6 octahedra alternate along the rock-salt [111] direction (i.e., there are alternating Na-O and Ti-O slabs) (Clarke et al., 1998). They evaluated its potential as a Na^+ insertion/extraction. This material delivers ∼75 mAh/g, corresponding to 0.3 Na^+, during multiple phases' transformation from O3 to O'3. It has an average sodium storage voltage of 1 V, while used as an anode in SIB. In 2014, Ceder et al. re-investigated O3-$NaTiO_2$ as an anode material for sodium-ion batteries (Wu et al., 2015a). Approximately 0.5

Na is reversibly intercalated in $NaTiO_2$, corresponding to a reversible capacity of 152 mAh/g. Special Na^+/vacancy ordering was observed and accompanied with an unusual lattice parameter variation, yielding a constant inter-slab distance and slight change in the in-plane Ti–Ti distance in the O'3 phase. The O3-type $Na_{0.8}Ni_{0.4}Ti_{0.6}O_2$ was investigated as an anode by Zhou and co-workers (Guo et al., 2015a). The reversible capacity of $Na_{0.8}Ni_{0.4}Ti_{0.6}O_2$ is 107 mAh/g with a distinct step around 0.7 V. $Na_{0.8}Ni_{0.4}Ti_{0.6}O_2$-based symmetric cell has a voltage of 2.8 V, a reversible discharge capacity of 85 mAh/g, 75% capacity retention after 150 cycles. In our opinion, the maximum sodium content in $Na_{0.8}Ni_{0.4}Ti_{0.6}O_2$ is 1, so insertion and extraction of 0.2 mol Na^+ corresponds to 52 mAh/g, and the extra capacities are attributed to the participation of conductive additives, such as carbon. Recently, the Hu Group reported an O3-type oxide with low sodium content, $Na_{0.66}Mg_{0.34}Ti_{0.66}O_2$, as an anode for sodium-ion batteries (Zhao et al., 2018a). This material delivers a capacity of about 98 mAh/g in a voltage range of 0.4–2.0 V and exhibits a better cycling stability (ca. 94.2 % of capacity retention after 128 cycles). *In-situ* XRD reveals a single-phase reaction in the discharge–charge process, which is different from the common phase transitions reported in O3-type electrodes; this single-phase mechanism ensures long-term cycling stability and high rate capacity.

Monoclinic $Na_2Ti_xO_{2x+1}$

$Na_2Ti_3O_7$

In 2011, Palacin et al. reported that $Na_2Ti_3O_7$ consisting of zigzag-type layers are formed by stacking TiO_6 octahedra ribbon, the Na^+ cations locate between the TiO_6 ribbons. $Na_2Ti_3O_7$ takes up 2 Na^+ in a formula unit at a low storage voltage of 0.3 V vs. Na^+/Na (Senguttuvan et al., 2011). The structure and electrochemical performance was shown in **Figure 2D**. However, the initial coulombic efficiency was rather low and only 10 cycles were shown. Hu et al. found that the sodium storage behavior was affected by the particle size of $Na_2Ti_3O_7$ (Pan et al., 2013b). A nano-sized $Na_2Ti_3O_7$ anode exhibited higher storage capacity than a micro-sized one. After optimization of the electrolyte and binder, the $Na_2Ti_3O_7$ electrode exhibited a reversible capacity of 188 mAh/g in 1 M NaFSI/PC electrolyte and sodium alginate as a binder at a current rate of 0.1C in a voltage range of 0.0–3.0 V. Unfortunately, the cycling properties are not satisfactory. In order to improve cycle life, $Na_2Ti_3O_7$@MWCNTs (Wei et al., 2014), $Na_2Ti_3O_7$/C (Ding et al., 2017), $Na_2Ti_3O_7$@N-Doped Carbon Hollow Spheres (Xie et al., 2017), $Na_2Ti_3O_7$/Titanium Peroxide (Zhao et al., 2015) and F-Doping $Na_2Ti_3O_7$ (Chen et al., 2018) were investigated. However, their performances were not satisfactory due to the low electronic conductivities and structural instability which needs to be further improved. In addition, full sodium-ion batteries have been tested based on advantageous electrochemical features of nanostructured $Na_2Ti_3O_7$. –for example, by using $VOPO_4$ material as a cathode, the full cell showed the operating voltages close to 2.9 V and delivered a reversible capacity of 114 mAh/g at a rate of 0.1C. It also shows outstanding rate capability (∼74 mA h/g at 2C rate) and excellent cycling stability (92.4% capacity retention after 100 cycles) (Li et al., 2016a).

$Na_2Ti_6O_{13}$

$Na_2Ti_6O_{13}$ crystallizes in a monoclinic crystalline structure with continuous tunnel channels along the *c* axis, offering space to accommodate the alkali metals (Dominko et al., 2006). In the crystal structure of $Na_2Ti_6O_{13}$, all of the oxygen atoms belong to at least two octahedra. Transformation of the crystal structure of $Na_2Ti_3O_7$ to that of $Na_2Ti_6O_{13}$ is described as a condensation of the two-dimensional layers of octahedra to a three-dimensional structure by sharing these one-coordinated oxygen atoms. It means that there is no terminal oxygen atom in the crystal structure of $Na_2Ti_6O_{13}$; all oxygen atoms are linearly coordinated by two titanium atoms. The TiO_6 octahedra in $Na_2Ti_6O_{13}$ are more regular, there are no very long or very short Ti-O distances. In 2011, T. Brousse et al. investigated $Na_2Ti_6O_{13}$ as the negative electrode for sodium-ion batteries (Trinh et al., 2012). The electrode showed a 0.8 V plateau vs. Na/Na^+, with an initial discharge capacity and initial columbic efficiency of only 22 mAh/g and 27%, respectively, Shen et al. subsequently performed DFT simulation and showed that a maximum of 4 Na^+ are inserted into this structure (Shen and Wagemaker, 2014). They obtained 196 mAh/g by lowering the cut-off voltage from 0.3 to 0 V.

$Na_2Ti_4O_9$

Kataoka et al. reported a tunnel-type $Na_2Ti_4O_9$ as a negative electrode for sodium-ion batteries (Kataoka and Akimoto, 2016). The crystal structure of $Na_2Ti_4O_9$ shows all of the TiO_6 octahedra are strongly distorted. The remarkably defective occupations for all of three sodium sites in the $Na_2Ti_4O_9$ sample; 72% for Na_1, 69% for Na_2 and 58% for Na_3 sites, should be noted. The electrochemical measurements of $Na_2Ti_4O_9$ showed the reversible sodium insertion and extraction reactions at 1.1 V, 1.5 V, and 1.8 V vs. Na/Na^+. The reversible capacity for the sodium cell was 100 mAh/g at a current density of 12 mA/g, which progressively faded to 45 mAh/g after 60 cycles.

$ATiOPO_4$ (A = NH_4, K, Na)

$KTiOPO_4$ is a well-known excellent non-linear optical material. Its crystal structure contains polytitanate chains interconnected by PO_4 tetrahedral units and belongs to the Pna21 space group; K^+ ions occupy two different sites, K1 and K2. The K1 site is located near the center of a passage and the K2 site is near the point of intersection of TiO_6 and PO_4, as shown in **Figure 2H**. The preparation of $NaTiOPO_4$ by the traditional solid-state reaction is difficult. Fortunately, it was found that $NaTiOPO_4$ is easily synthesized using a hydrothermal method and $KTiOPO_4$ can be prepared by ion-exchange of K^+ with NH_4^+ and Na^+ due to the difference in their ionic radii. These materials were investigated by electrochemical discharge/charge, with average charge voltages of 1.45 V ($NH4TiOPO_4$), 1.4 V ($KTiOPO_4$), and 1.5 V ($NaTiOPO_4$), and capacities of 100 mAh/g ($NH4TiOPO_4$), 60 mAh/g ($KTiOPO_4$), 80 mAh/g ($NaTiOPO_4$), respectively (Mu et al., 2016). *In-situ* XRD was performed to understand the reaction, and the results revealed a bi-phase reaction mechanism in $NaTiOPO_4$ during sodium intercalation and de-intercalation.

NASICON Compounds

The crystal structure of NASICON compounds was determined in 1968. In general, the NASICON-type compounds ($Na_xM1M2(XO_4)_3$ (M = V, Ti, Fe, Tr or Nb etc.; X = P, or S, x = 0–4) exhibit an open three-dimensional structure with two types of interstitial positions (*M1, M2*), where the conductor cations are distributed. The matrix can be broken down into fundamental groups of $2MO_6$ octahedra separated by 3 XO_4 tetrahedra that share common corner oxygen's. As there are no shared edges or shared faces in the matrix, all of the large sodium sites are connected. The NASICON-type $NaTi_2(PO_4)_3$ (shown in **Figure 2I**) exhibits a reversible Na storage capacity of ca.120 mAh/g at ca. 2.1 V vs. Na^+/Na via Ti^{4+}/Ti^{3+} conversion (Park et al., 2011). The storage voltage is high for organic sodium-ion batteries, but suitable for aqueous ion batteries. Reported examples of NASICON compounds include $Na_{0.44}MnO_2/NaTi_2(PO_4)_3$ (Kim et al., 2013), $Na_2CuFe(CN)_6/NaTi_2(PO4)_3$ (Wessells et al., 2011a), $Na_2NiFe(CN)_6/ NaTi_2(PO4)_3$ (Wessells et al., 2011b), $Na_3V_2(PO_4)_3/ NaTi_2(PO_4)_3$ (Song et al., 2014).

The discussion above demonstrates that the sodium storage voltages of Ti- containing anodes depend on their crystal structures, especially the local environments of Ti ions, although the redox reaction always involving Ti^{4+} and Ti^{3+}. Their structures, voltages and electrochemical performances are summarized in **Figure 3A** in the order of voltage increase.

The average Na^+ ion insertion potentials of electrode materials can also be estimated by Density Function Theory calculation which plays an important role in new material design. The equilibrium intercalation voltage depends on the chemical potential difference of sodium in the electrode materials and can be approximated by equation (1) without considering the small contributions of entropy and volume changes to the cell voltage (Aydinol and Ceder, 1997; Meng and Arroyo-De Dompablo, 2009).

$$V_{ave} = \frac{E_{total}\,(Na_{x2}\,final) - \left[E_{total}\,(Na)_{x1}\,pristine\right) + (x_2 - x_1)E_{total}(Na)}{(x_2 - x_1)\,z\,F} \tag{1}$$

where x_1 and x_2 are the Na^+ contents in the pristine and final electrodes; F is the Faraday constant; z is electronic charge of sodium ions, i.e., 1; E_{total} is the total energy per formula unit which is a function of the crystal structure. In the above mentioned Ti containing compounds, despite all Ti ions situated at the center of TiO_6 octahedra, the differences in the connections between TiO_6 octahedra as well as between TiO_6 and other components constitute the different environments of Ti in various structures, as a consequence, the total energies are different, and therefore have different average cell voltages. For example, $Na_{0.66}[Li_{0.22}Ti_{0.78}]O_2$ (0.47 V), $Li_4Ti_5O_{12}$ (0.91 V), Na2Ti3O7 (0.3 V) (Rousse et al., 2013). In general, Ti-containing anodes have low electronic conductivity. Among the six structures mentioned in this section, layered oxides showed good cycle life due to their single-phase reaction mechanism and low volume change, but their capacities must increase from the present value of ca. 100 mAh/g. Therefore, future work should focus on increasing the capacities (200–300 mAh/g) and electronic conductivities of the "zero strain" layered oxides with storage voltages at ca. 1 V.

FUNCTION OF TI IN THE CATHODE

In contrast to the anode, the cathode materials include the redox couples $Ni^{2+}/Ni^{3+}/Ni^{4+}$, $Mn^{2+}/Mn^{3+}/Mn^{4+}$, Co^{3+}/Co^{4+}, V^{3+}/V^{4+}, Cu^{2+}/Cu^{3+}, Cr^{3+}/Cr^{4+}, etc. Although Ti^{4+}-dopant does not participate in charge transfer involving Na^+ extraction and insertion, it affects the crystal structure, including cation-ordering and lattice structure.

Structure Change

In the case of P2-type materials, the value of "x" in Na_xMO_2 is typically 2/3, leaving many vacancies in the alkali layer. Na_xMnO_2 ($0.6 < \times < 0.72$) is a typical P2-layered oxide. Caballero reported a layered sodium manganese oxide ($Na_{0.6}MnO_2$) synthesized by a sol–gel method (Caballero et al., 2002). This material delivered a constant specific capacity of 140 mAh/g at 0.1 mA/cm^2 in a voltage window of 2.0–3.8V. However, the continuous strains and distortions resulting from insertion and extraction of Na^+ caused the host structure to gradually collapse and yielded an amorphous material after eight cycles. This led to a progressive reduction of the cell capacity, regardless of the voltage window used. In 2014, DFT calculations by Ceder et al. revealed that Na^+ ordering in Na_xMnO_2 was controlled by the underlying combination of electrostatic and electronic structure interactions via Jahn–Teller effect, enabling some Na to occupy the highly distorted octahedral site. This led to Na and Mn charge-ordered stripes, which yielded a fascinating low-temperature magnetic ordering (Li et al., 2014). In 2015, Wang et al. reported a tunnel-type structure, $Na_x[Mn_xTi_{1-x}]O_2$ (x = 0.44, 0.50, 0.55, 0.60, 0.63, 0.66), which has a large S-shaped tunnel and a small hexagonal tunnel formed by MnO_6 and MnO_5 polyhedrals (Wang et al., 2015b). The structure of these materials was similar to tunnel-type $Na_{0.44}MnO_2$ (S.G.: Pbam) (as shown in **Figure 3B**) with sodium ions in the S-shaped and hexagonal tunnels. Unlike layered Na_xMnO_2, tunnel-type $Na_x[Mn_xTi_{1-x}]O_2$ is stable in an aqueous solution. Hence, $Na_{0.66}[Mn_{0.66}Ti_{0.34}]O_2$ can be used as a positive electrode material for aqueous sodium-ion batteries. In particular, it showed the highest reversible capacity (76 mAh/g) at a current rate of 2C among all the oxide electrode materials, with an average operating voltage of 1.2 V when coupled with a $NaTi_2(PO_4)_3$/C negative electrode. The $Na_{0.66}[Mn_{0.66}Ti_{0.34}]O_2|NaTi_2(PO_4)_3$/C aqueous sodium-ion cell demonstrates excellent cycle performance with minimal capacity decay after 300 cycles.

The O3-type $NaFeO_2$ attracted a lot of attention due to its inexpensive and non-toxic features, and is expected to have a reversible Fe^{4+}/Fe^{3+} conversion (Yabuuchi et al., 2012). Recent studies showed a reversible Na storage in $NaFeO_2$ at 3.3 V with a small polarization by limiting the cut-off voltage. In contrast, the Li analog, O3-$LiFeO_2$ (Kanno et al., 1996), is nearly electrochemically inactive due to a low energy barrier for Fe^{4+} migrating to the alkali layer. The charge capacity in the half cell was ascribed to the dominant reaction of oxygen

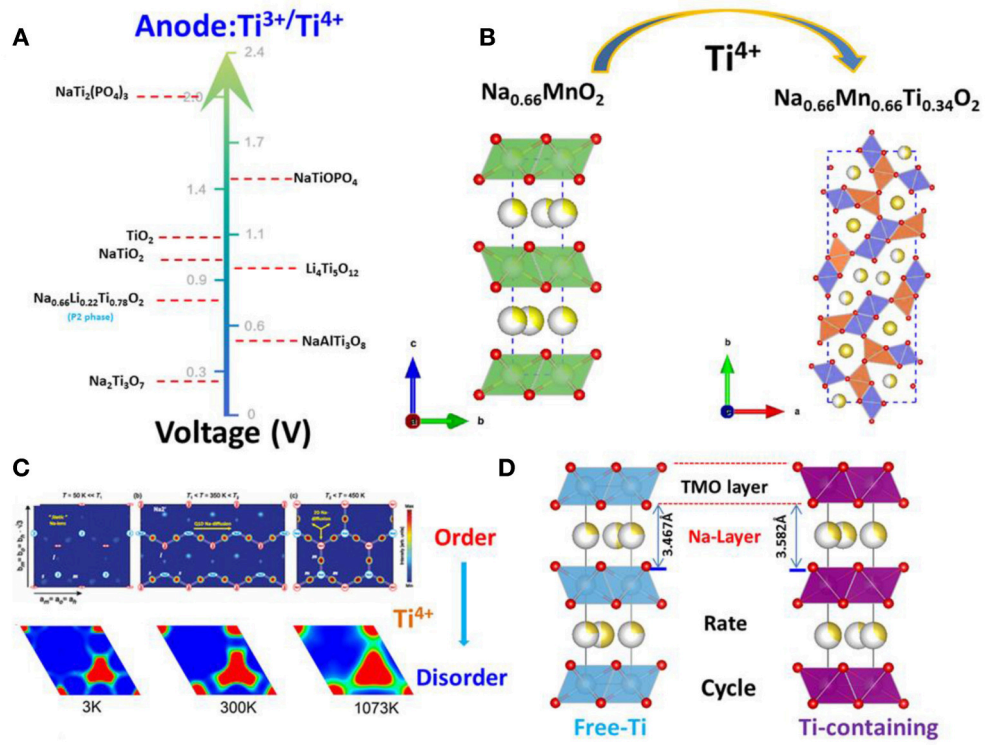

FIGURE 3 | Roles of Ti in the electrodes. **(A)** The voltage of Ti^{3+}/Ti^{4+} in the different structure as anode for sodium-ion batteries; **(B)** Ti-doping resulting in the structure change from the P2-layered to tunnel-type. **(C)** Upper: For the three temperature regions, there is a clear evolution from static Na+ ions to quasi-1D ion diffusion along *a* axis to finally fully 2D ion diffusion; With permission from APS. Lower: The mean square displacements (MSDs) of Na+ ions in P2-$Na_{0.6}[Cr_{0.6}Ti_{0.4}]O_2$ are displayed at 1,200, 1,500, 1,800, 2,400, and 2,700 K; With permission from Springer. **(D)** The schematic diagram of Ti-substitution increases the crystal lattice of P2-layered oxides.

removal at the solid/electrolyte interface rather than Fe^{4+}/Fe^{3+} conversion as the Fe^{3+} 3d-orbital is strongly hybridized with the oxygen 2p orbital in the Li system; oxygen removal is more favorable energetically than the oxidation to Fe^{4+}. Substitution of Ti for Fe in $NaFeO_2$ changes the structure from the O3-phase to a tunnel type. For example, the tunnel-type $Na_{0.875}Fe_{0.875}Ti_{1.125}O_4$ delivered a capacity of 45 mAh/g corresponding to the extraction/insertion of 0.37 Na^+ ions. Compared to $NaFeO_2$, $Na_{0.875}Fe_{0.875}Ti_{1.125}O_4$ exhibits the low capacities due to the lower quantity of sodium participates in the redox reaction, but the sodium storage voltage improves from 3.2 to 3.6 V (Pan et al., 2013a; Bhange et al., 2017).

Cation-Disorder

Na_xCoO_2 is known as the first layered oxide investigated as a Na intercalation host (Delmas et al., 1981). Depending on the sodium content and temperature of this compound, an interplay between Na^+-Na^+ and Na^+-$Co^{3+/4+}$ electrostatic interactions coupled with $Co^{3+/4+}$ charge ordering results in the formation of numerous Na^+/vacancy-ordered superstructures (see the **Figure 3C**; Medarde et al., 2013). These ordered superstructures have distinct voltage plateaus, lowering the Na^+ ion diffusion coefficient and even reducing the dimensionality of ionic transport. The combination of these characteristics, in turn, result in rapid capacity-fading during cycling, as in the case of Na_xCoO_2 (Berthelot et al., 2011), Na_xMnO_2 (Jeong and Manthiram, 2001), Na_xVO_2 (Guignard et al., 2013), $Na_{2/3}Ni_{1/3}Mn_{2/3}O_2$ (Lu and Dahn, 2001), and $Na_{2/3}Co_{2/3}Mn_{1/3}O_2$ (Carlier et al., 2011). In 2015, Wang et al. reported a critical difference in ionic radii between M1 and M2 is ∼15% in layered oxides P2-$NaM1M2O_2$ (M1, M2 are transitional metals) which governs cation order-disorder transition (Wang et al., 2015c). If the radius difference is higher than 15% and M1/M2 content is close to a rational ratio, then an ordered structure is expected; otherwise M1 and M2 is disordered. The presence of charge ordering is determined by the redox potentials (that is, Fermi level of M1 and M2). Small differences are favorable for charge ordering, even if M1 and M2 are chemically disordered. Finally, Na^+/vacancy ordering and charge ordering are coupled to each other. There would be no charge ordering without Na^+/vacancy ordering and vice versa. The ratio of ionic radii of Ti^{4+}/Ni^{2+}, Ti^{4+}/Co^{2+}, Ti^{4+}/Cr^{3+}, Ti^{4+}/Mn^{3+} are 1.14, 1.04, 1.02, 1.14, respectively, which are <1.15. This means that the transition layered oxides are all disordered. In addition, there are large differences in redox potentials (or Fermi level) of Ti^{4+}/Ni^{2+}, Ti^{4+}/Co^{2+}, Ti^{4+}/Cr^{3+},

Ti^{4+}/Mn^{3+} which leads to charge disordering, and hence Na^+/vacancy disordering. The behavior of charge/discharge profiles of $Na_{2/3}Ni_{1/3}Ti_{2/3}O_2$ (Shanmugam and Lai, 2014), $Na_{2/3}Co_{1/3}Ti_{2/3}O_2$ (Guo et al., 2015b) and $Na_{0.6}Cr_{0.6}Ti_{0.4}O_2$ exhibit a smooth slope without the plateau that is attributed to the Na^+/vacancy ordering. Wang et al. analyzed neutron powder diffraction data collected from $Na_{0.6}[Cr_{0.6}Ti_{0.4}]O_2$ on cooling to 3 K; the results showed no evidence of Cr/Ti and Na+/vacancy orderings, and charge and Na^+/vacancy orderings were also not observed in the tunnel-type Ti-substituted $Na_{0.44}MnO_2$ In contrast, Na^+/vacancy ordering was found in $Na_{0.7}CoO_2$ which exhibits the different transport channels at the different temperatures (see in **Figure 3C**).

Distance Between Layers

A larger crystal lattice enhances ionic transport of Na^+, thus improving rate and cycle performance (As shown in **Figure 3D**). Normally, Ti-doping will lead to an increase in the alkali-layer distance of 1–3%, such as in $NaCrO_2$ (Li et al., 2019), $Na_{2/3}CoO_2$ (Sabi et al., 2017) and $Na_{0.67}Fe_{0.5}Mn_{0.5}O_2$ (Park et al., 2018). Recently, Lee et al. reported enhanced rate capability and cycle performance by substitution of Ti for Fe in P2-Type $Na_{0.67}Fe_{0.5}Mn_{0.5}O_2$ cathode for sodium-ion batteries (Park et al., 2018). They found 5% Ti substitution increases the crystal lattice from 3.528 to 3.571 Å. This small change promotes Na-ion diffusion and prevents the phase transition from the P2 to the OP4/"Z" structure. In addition, Du's group reported that with 5% Ti-substitution in $NaCrO_2$, the crystal lattice expanded 1%, which resulted in an increase of 25% in capacity retention at the current rate of 30C and enhancement in cycle life (Li et al., 2019).

SUMMARY

The role of Ti in the cathode and anode for sodium-ion batteries are reviewed in the present work. In the anode, the redox couple, Ti^{4+}/Ti^{3+}, exhibits different storage voltages and imparted properties that are beneficial in designing different materials for various applications, such as $NaTi_2(PO_4)_3$ for aqueous batteries, P2-$Na_{0.66}Li_{0.22}Ti_{0.78}O_2$ for long cycle batteries, etc. The substitution of Ti disrupts the structure ordering and expands the crystal lattice which prolongs the cycle life and enhances rate performance. In addition, Ti-substituted $Na_{2/3}MnO_2$ prevents H_3O^+ intercalation, making it a perfect cathode material for aqueous sodium-ion batteries. Developing practical cathode and anode materials for sodium-ion batteries is a big challenge. In spite of the advances discussed in this review, there is still substantial room for further improvement.

Although the above-mentioned challenges still remain, the recent progress in the development of Ti-compounds is significant. There is now an improved understanding of the effects of Ti addition on the crystal structure, including the lattice expansion and distortion, the cation and vacancy orderings, as well as on the electronic configurations of the redox couples. This knowledge helps researchers to identify other dopants and materials for designing and developing new high-performance electrode materials. We believe that further studies will lead to more exciting results. This review highlights the importance of designing and exploring disordered transition metal/charge in electrodes as an effective strategy to improve Na-storage properties, including rate capacity, cycle stability and high-power performance.

AUTHOR CONTRIBUTIONS

YW wrote the draft. All authors contributed to the writing, discussion, and revision of the final version.

FUNDING

Centre d'excellence en électrification des transports et stockage d'énergie, Québec, Canada.

REFERENCES

Alcántara, R., Jiménez-Mateos, J. M., Lavela, P., and Tirado, J. L. (2001). Carbon black: a promising electrode material for sodium-ion batteries. *Electrochem. Commun.* 3, 639–642. doi: 10.1016/S1388-2481(01)00244-2

Armand, M., and Tarascon, J. M. (2008). Building better batteries. *Nature* 451, 652–657. doi: 10.1038/451652a

Aydinol, M. K., and Ceder, G. (1997). First-principles prediction of insertion potentials in Li-Mn oxides for secondary Li batteries. *J. Electrochem. Soc.* 144, 3832–3835. doi: 10.1149/1.1838099

Berthelot, R., Carlier, D., and Delmas, C. (2011). Electrochemical investigation of the P2-NaxCoO_2 phase diagram. *Nat. Mater.* 10, 74–U73. doi: 10.1038/nmat2920

Bhange, D. S., Ali, G., Kim, J-Y., Chung, K. Y., and Nam, K-W. (2017). Improving the sodium storage capacity of tunnel structured $Na_xFe_xTi_{2-x}O_4$ (x = 1, 0.9 & 0.8) anode materials by tuning sodium deficiency. *J. Power Sources* 366, 115–122. doi: 10.1016/j.jpowsour.2017.08.112

Braconnier, J. J., Delmas, C., and Hagenmuller, P. (1982). Etude par desintercalation electrochimique des systemes Na_xCrO_2 et Na_xNiO_2. *Mater. Res. Bull.* 17, 993–1000. doi: 10.1016/0025-5408(82)90124-6

Caballero, A., Hernan, L., Morales, J., Sanchez, L., Pena, J. S., and Aranda, M., (2002). Synthesis and characterization of high-temperature hexagonal P2-$Na_{0.6}MnO_2$ and its electrochemical behaviour as cathode in sodium cells. *J. Mater. Chem.* 12, 1142–1147. doi: 10.1039/b108830k

Carlier, D., Cheng, J. H., Berthelot, R., Guignard, M., Yoncheva, M., Stoyanova, R., et al. (2011). The P2-$Na_{2/3}Co_{2/3}Mn_{1/3}O_2$ phase: structure, physical properties and electrochemical behavior as positive electrode in sodium battery. *Dalton Transact.* 40, 9306–9312. doi: 10.1039/c1dt10798d

Chen, C., Vaughey, J., Jansen, A., Dees, D., Kahaian, A., Goacher, T., et al. (2001). Studies of Mg-substituted $Li_{4-x}Mg_xTi_5O_{12}$ spinel electrodes ($0 \leq x \leq 1$) for lithium batteries. *J. Electrochem. Soc.* 148, A102–A104. doi: 10.1149/1.1344523

Chen, J., Song, W., Hou, H., Zhang, Y., Jing, M., Jia, X., et al. (2015). Ti^{3+} Self-doped dark rutile TiO_2 ultrafine nanorods with durable high-rate capability for lithium-ion batteries. *Adv. Funct. Mater.* 25, 6793–6801. doi: 10.1002/adfm.201502978

Chen, Z., Lu, L., Gao, Y., Zhang, Q., Zhang, C., Sun, C., et al. (2018). Effects of F-doping on the electrochemical performance of $Na_2Ti_3O_7$ as an anode for sodium-ion batteries. *Materials* 11:2206. doi: 10.3390/ma11112206

Chevrier, V. L., and Ceder, G. (2011). Challenges for Na-ion negative electrodes. *J. Electrochem. Soc.* 158, A1011–A1014. doi: 10.1149/1.3607983

Clarke, S. J., Fowkes, A. J., Harrison, A., Ibberson, R. M., and Rosseinsky, M. J. (1998). Synthesis, structure, and magnetic properties of $NaTiO_2$. *Chem. Mater.* 10, 372–384. doi: 10.1021/cm970538c

Darwiche, A., Marino, C., Sougrati, M. T., Fraisse, B., Stievano, L., and Monconduit, L. (2012). Better cycling performances of bulk Sb in Na-ion batteries compared to Li-ion systems: an unexpected electrochemical mechanism. *J. Am. Chem. Soc.* 134, 20805–20811. doi: 10.1021/ja310347x

Delmas, C., Braconnier, J-J., Fouassier, C., and Hagenmuller, P. (1981). Electrochemical intercalation of sodium in $NaxCoO_2$ bronzes. solid state ionics 3–4, 165–169. doi: 10.1016/0167-2738(81)90076-X

Delmas, C., Fouassier, C., and Hagenmuller, P. (1980). Structural classification and properties of the layered oxides. *Physica B C* 99, 81–85. doi: 10.1016/0378-4363(80)90214-4

Ding, C., Nohira, T., and Hagiwara, R. (2017). Electrochemical performance of Na2Ti3O7/C negative electrode in ionic liquid electrolyte for sodium secondary batteries. *J. Power Sources* 354, 10–15. doi: 10.1016/j.jpowsour.2017.04.027

Doeff, M. M., Peng, M. Y., Ma, Y. P., and Dejonghe, L. C. (1994). Orthorhombic $NaxMnO_2$ as a cathode material for secondary sodium and lithium polymer batteries. *J. Electrochem. Soc.* 141, L145–L147. doi: 10.1149/1.2059323

Dominko, R., Baudrin, E., Umek, P., Arčon, D., Gaberšček, M., and Jamnik, J. (2006). Reversible lithium insertion into $Na_2Ti_6O_{13}$ structure. *Electrochem. Commun.* 8, 673–677. doi: 10.1016/j.elecom.2006.02.017

Dunn, B., Kamath, H., and Tarascon, J-M. (2011). Electrical energy storage for the grid: a battery of choices. *Science* 334, 928–935. doi: 10.1126/science.1212741

Ellis, B. L., and Nazar, L. F. (2012). Sodium and sodium-ion energy storage batteries. *Curr. Opin. Solid State Mater. Sci.* 16, 168–177. doi: 10.1016/j.cossms.2012.04.002

Farbod, B., Cui, K., Kalisvaart, W. P., Kupsta, M., Zahiri, B., Kohandehghan, A., et al. (2014). Anodes for sodium ion batteries based on tin-germanium-antimony alloys. *Acs Nano* 8, 4415–4429. doi: 10.1021/nn4063598

Ferg, E., Gummow, R., De Kock, A., and Thackeray, M. (1994). Spinel anodes for lithium-ion batteries. *J. Electrochem. Soc.* 141, L147–L150. doi: 10.1149/1.2059324

Fielden, R., Cole, L., and Obrovac, M. N. (2017). Low voltage sodium intercalation in $Na_xV_xTi_{1-x}O_2$ ($2/3 \leq x \leq 1$). *J. Electrochem. Soc.* 164, A490–A497. doi: 10.1149/2.1361702jes

González, J. R., Alcántara, R., Nacimiento, F., Ortiz, G. F., and Tirado, J. L. (2014). Microstructure of the epitaxial film of anatase nanotubes obtained at high voltage and the mechanism of its electrochemical reaction with sodium. *CrystEngComm* 16, 4602–4609. doi: 10.1039/C4CE00272E

Goodenough, J. B., and Kim, Y. (2009). Challenges for rechargeable Li batteries. *Chem. Mater.* 22, 587–603. doi: 10.1021/cm901452z

Gover, R. K. B., Bryan, A., Burns, P., and Barker, J. (2006). The electrochemical insertion properties of sodium vanadium fluorophosphate, $Na_3V_2(PO_4)_2F_3$. *Solid State Ionics* 177, 1495–1500. doi: 10.1016/j.ssi.2006.07.028

Guignard, M., Didier, C., Darriet, J., Bordet, P., Elkaïm, E., and Delmas, C. (2013). P_2-$NaxVO_2$ system as electrodes for batteries and electron-correlated materials. *Nat. Mater.* 12, 74–80. doi: 10.1038/nmat3478

Guo, S., Yu, H., Liu, P., Ren, Y., Zhang, T., Chen, M., et al. (2015a). High-performance symmetric sodium-ion batteries using a new, bipolar O3-type material, $Na_{0.8}Ni_{0.4}Ti_{0.6}O_2$. *Energy Environ. Sci.* 8, 1237–1244. doi: 10.1039/C4EE03361B

Guo, S. S., Liu, P., Sun, Y., Zhu, K., Yi, J., Chen, M. W., et al. (2015b). A high-voltage and ultralong-life sodium full cell for stationary energy storage. *Angew. Chem. Int. Ed.* 54, 11701–11705. doi: 10.1002/anie.201505215

He, H., Gan, Q., Wang, H., Xu, G-L., Zhang, X., Huang, D., et al. (2018). Structure-dependent performance of TiO_2/C as anode material for Na-ion batteries. *Nano Energy* 44, 217–227. doi: 10.1016/j.nanoen.2017.11.077

He, H., Sun, D., Zhang, Q., Fu, F., Tang, Y., Guo, J., et al. (2017). Iron-doped cauliflower-like rutile TiO_2 with superior sodium storage properties. *ACS Appl. Mater. Interfaces* 9, 6093–6103. doi: 10.1021/acsami.6b15516

Hosono, E., Saito, T., Hoshino, J., Okubo, M., Saito, Y., Nishio-Hamane, D., et al. (2012). High power Na-ion rechargeable battery with single-crystalline $Na_{0.44}MnO_2$ nanowire electrode. *J. Power Sources* 217, 43–46. doi: 10.1016/j.jpowsour.2012.05.100

Hu, Z., Wang, L., Zhang, K., Wang, J., Cheng, F., Tao, Z., et al. (2014). MoS_2 nanoflowers with expanded interlayers as high-performance anodes for sodium-ion batteries. *Angew. Chem. Int. Ed.* 53, 12794–12798. doi: 10.1002/anie.201407898

Jeong, Y. U., and Manthiram, A. (2001). Synthesis of $Na_xMnO_{2+\delta}$ by a reduction of aqueous sodium permanganate with sodium iodide. *J. Solid State Chem.* 156, 331–338. doi: 10.1006/jssc.2000.9003

Jian, Z., Zhao, B., Liu, P., Li, F., Zheng, M., Chen, M., et al. (2014). Fe_2O_3 nanocrystals anchored onto graphene nanosheets as the anode material for low-cost sodium-ion batteries. *Chem. Commun.* 50, 1215–1217. doi: 10.1039/C3CC47977C

Jian, Z., Zhao, L., Pan, H., Hu, Y-S., Li, H., Chen, W., et al. (2012). Carbon coated $Na_3V_2(PO_4)_3$ as novel electrode material for sodium ion batteries. *Electrochem. Commun.* 14, 86–89. doi: 10.1016/j.elecom.2011.11.009

Kanno, R., Shirane, T., Kawamoto, Y., Takeda, Y., Takano, M., Ohashi, M., et al. (1996). Synthesis, structure, and electrochemical properties of a new lithium iron oxide, $LiFeO_2$, with a corrugated layer structure. *J. Electrochem. Soc.* 143, 2435–2442. doi: 10.1149/1.1837027

Kataoka, K., and Akimoto, J. (2016). Synthesis and electrochemical sodium and lithium insertion properties of sodium titanium oxide with the tunnel type structure. *J. Power Sources* 305, 151–155. doi: 10.1016/j.jpowsour.2015.11.090

Kim, D. J., Ponraj, R., Kannan, A. G., Lee, H-W., Fathi, R., Ruffo, R., et al. (2013). Diffusion behavior of sodium ions in $Na_{0.44}MnO_2$ in aqueous and non-aqueous electrolytes. *J. Power Sources* 244, 758–763. doi: 10.1016/j.jpowsour.2013.02.090

Kim, J., Seo, D-H., Kim, H., Park, I., Yoo, J-K., Jung, S-K., et al. (2015). Unexpected discovery of low-cost maricite $NaFePO_4$ as a high-performance electrode for Na-ion batteries. *Energy Environ. Sci.* 8, 540–545. doi: 10.1039/C4EE03215B

Kim, K-T., Ali, G., Chung, K. Y., Yoon, C. S., Yashiro, H., Sun, Y-K., et al. (2014). Anatase titania nanorods as an intercalation anode material for rechargeable sodium batteries. *Nano Lett.* 14, 416–422. doi: 10.1021/nl402747x

Lan, T., Wang, T., Zhang, W., Wu, N-L., and Wei, M. (2017). Rutile TiO_2 mesocrystals with tunable subunits as a long-term cycling performance anode for sodium-ion batteries. *J. Alloys Compd.* 699, 455–462. doi: 10.1016/j.jallcom.2016.12.337

Li, H., Peng, L., Zhu, Y., Chen, D., Zhang, X., and Yu, G. (2016a). An advanced high-energy sodium ion full battery based on nanostructured $Na_2Ti_3O_7$/$VOPO_4$ layered materials. *Energy Environ. Sci.* 9, 3399–3405. doi: 10.1039/C6EE00794E

Li, J., Liu, J., Sun, Q., Banis, M. N., Sun, X., and Sham, T-K. (2017). Tracking the effect of sodium insertion/extraction in amorphous and anatase TiO_2 nanotubes. *J. Phys. Chem. C* 121, 11773–11782. doi: 10.1021/acs.jpcc.7b01106

Li, W., Wang, Y., Hu, G., Peng, Z., Cao, Y., Zeng, Y., et al. (2019). Ti-doped $NaCrO_2$ as cathode materials for sodium-ion batteries with excellent long cycle life. *J. Alloys Compd.* 779, 147–155. doi: 10.1016/j.jallcom.2018.11.257

Li, X., Ma, X., Su, D., Liu, L., Chisnell, R., Ong, S. P., et al. (2014). Direct visualization of the jahn–teller effect coupled to Na ordering in $Na_{5/8}MnO_2$. *Nat. Mater.* 13:586. doi: 10.1038/nmat3964

Li, Y., Hu, Y-S., Li, H., Chen, L., and Huang, X. (2016b). A superior low-cost amorphous carbon anode made from pitch and lignin for sodium-ion batteries. *J Mater. Chem. A* 4, 96–104. doi: 10.1039/C5TA08601A

Li, Y., Xu, S., Wu, X., Yu, J., Wang, Y., Hu, Y-S., et al. (2015). Amorphous monodispersed hard carbon micro-spherules derived from biomass as a high performance negative electrode material for sodium-ion batteries. *J. Mater. Chem. A* 3, 71–77. doi: 10.1039/C4TA05451B

Li, Z., Young, D., Xiang, K., Carter, W. C., and Chiang, Y-M. (2013). Towards high power high energy aqueous sodium-ion batteries: the $NaTi_2(PO_4)_3$/$Na_{0.44}MnO_2$ system. *Adv. Energy Mater.* 3, 290–294. doi: 10.1002/aenm.201200598

Lim, S. Y., Lee, J. H., Kim, S., Shin, J., Choi, W., Chung, K. Y., et al. (2017). Lattice water for the enhanced performance of amorphous iron phosphate in sodium-ion batteries. *ACS Energy Lett.* 2, 998–1004. doi: 10.1021/acsenergylett.7b00120

Liu, Y., Wang, H., Cheng, L., Han, N., Zhao, F., Li, P., et al. (2016). TiS_2 nanoplates: a high-rate and stable electrode material for sodium ion batteries. *Nano Energy* 20, 168–175. doi: 10.1016/j.nanoen.2015.12.028

Lu, Y., Zhao, C., Qi, X., Qi, Y., Li, H., Huang, X., et al. (2018). Pre-oxidation-tuned microstructures of carbon anodes derived from pitch for enhancing Na storage performance. *Adv. Energy Mater.* 8:1800108. doi: 10.1002/aenm.201800108

Lu, Z., and Dahn, J. R. (2001). *In situ* x-ray diffraction study of P 2 - $Na_{2/3}$ $[Ni_{1/3}Mn_{2/3}]O_2$. *J. Electrochem. Soc.* 148, A1225–A1229. doi: 10.1149/1.1407247

Maazaz, A., Delmas, C., and Hagenmuller, P. (1983). A study of the $NaxTiO_2$ system by electrochemical deintercalation. *J. Inclus. Phenom.* 1, 45–51. doi: 10.1007/BF00658014

Medarde, M., Mena, M., Gavilano, J. L., Pomjakushina, E., Sugiyama, J., Kamazawa, K., et al. (2013). 1D to 2D Na+ion diffusion inherently linked to structural transitions in $Na_{0.7}CoO_2$. *Phys. Rev. Lett.* 110:266401. doi: 10.1103/PhysRevLett.110.266401

Meng, Y. S., and Arroyo-De Dompablo, M. E. (2009). First principles computational materials design for energy storage materials in lithium ion batteries. *Energy Environ. Sci.* 2, 589–609. doi: 10.1039/b901825e

Miyazaki, S., Kikkawa, S., and Koizumi, M. (1983). Chemical and electrochemical deintercalations of the layered compounds $LiMO_2$ (M = Cr, Co) and $NaMO_2$ (M=Cr, Fe, Co, Ni). *Synth. Met.* 6, 211–217. doi: 10.1016/0379-6779(83)90156-X

Mizushima, K., Jones, P. C., Wiseman, P. J., and Goodenough, J. B. (1980). $LixCoO_2$ ($0<x<1$): a new cathode material for batteries of high energy density. *Mater. Res. Bull.* 15, 783–789. doi: 10.1016/0025-5408(80)90012-4

Mu, L., Ben, L., Hu, Y-S., Li, H., Chen, L., and Huang, X. (2016). Novel 1.5 V anode materials, $ATiOPO_4$ (A = NH4, K, Na), for room-temperature sodium-ion batteries. *J. Mater. Chem. A* 4, 7141–7147. doi: 10.1039/C6TA00891G

Newman, G. H., and Klemann, L. P. (1980). Ambient temperature cycling of an Na - TiS_2 cell. *J. Electrochem. Soc.* 127, 2097–2099. doi: 10.1149/1.2129353

Oh, S-M., Myung, S-T., Hassoun, J., Scrosati, B., and Sun, Y-K. (2012). Reversible $NaFePO_4$ electrode for sodium secondary batteries. *Electrochem. Commun.* 22, 149–152. doi: 10.1016/j.elecom.2012.06.014

Pan, H., Hu, Y-S., and Chen, L. (2013a). Room-temperature stationary sodium-ion batteries for large-scale electric energy storage. *Energy Environ. Sci.* 6, 2338–2360. doi: 10.1039/c3ee40847g

Pan, H. L., Lu, X., Yu, X. Q., Hu, Y. S., Li, H., Yang, X. Q., et al. (2013b). Sodium storage and transport properties in layered $Na_2Ti_3O_7$ for room-temperature sodium-ion batteries. *Adv. Energy Mater.* 3, 1186–1194. doi: 10.1002/aenm.201300139

Pang, G., Yuan, C., Nie, P., Ding, B., Zhu, J., and Zhang, X. (2014). Synthesis of NASICON-type structured $NaTi_2(PO_4)_3$-graphene nanocomposite as an anode for aqueous rechargeable Na-ion batteries. *Nanoscale* 6, 6328–6334. doi: 10.1039/C3NR06730K

Park, J-K., Park, G-G., Kwak, H. H., Hong, S-T., and Lee, J-W. (2018). Enhanced rate capability and cycle performance of titanium-substituted P2-Type $Na_{0.67}Fe_{0.5}Mn_{0.5}O_2$ as a cathode for sodium-ion batteries. *ACS Omega* 3, 361–368. doi: 10.1021/acsomega.7b01481

Park, S. I., Gocheva, I., Okada, S., and Yamaki, J-I. (2011). Electrochemical properties of $NaTi_2(PO_4)_3$ Anode for rechargeable aqueous sodium-ion batteries. *J. Electrochem. Soc.* 158, A1067–A1070. doi: 10.1149/1.3611434

Ramireddy, T., Xing, T., Rahman, M. M., Chen, Y., Dutercq, Q., Gunzelmann, D., et al. (2015). Phosphorus–carbon nanocomposite anodes for lithium-ion and sodium-ion batteries. *J. Mater. Chem. A* 3, 5572–5584. doi: 10.1039/C4TA06186A

Reddy, R. N., and Reddy, R. G. (2004). Synthesis and electrochemical characterization of amorphous MnO_2 electrochemical capacitor electrode material. *J. Power Sources* 132, 315–320. doi: 10.1016/j.jpowsour.2003.12.054

Rousse, G., Arroyo-De Dompablo, M. E., Senguttuvan, P., Ponrouch, A., Tarascon, J-M., and Palacín, M. R. (2013). Rationalization of intercalation potential and redox mechanism for $A_2Ti_3O_7$ (A = Li, Na). *Chem. Mater.* 25, 4946–4956. doi: 10.1021/cm4032336

Sabi, N., Sarapulova, A., Indris, S., Ehrenberg, H., Alami, J., and Saadoune, I. (2017). Effect of titanium substitution in a a P2-$Na_{2/3}Co_{0.95}Ti_{0.05}O_2$ Cathode material on the structural and electrochemical properties. *ACS Appl. Mater. Interfaces* 9, 37778–37785. doi: 10.1021/acsami.7b11636

Samin, A., Kurth, M., and Cao, L. (2015). Ab initio study of radiation effects on the $Li_4Ti_5O_{12}$ electrode used in lithium-ion batteries. *AIP Adv.* 5:47110. doi: 10.1063/1.4917308

Senguttuvan, P., Rousse, G., Seznec, V., Tarascon, J-M., and Palacín, M. R. (2011). $Na_2Ti_3O_7$: Lowest voltage ever reported oxide insertion electrode for sodium ion batteries. *Chem. Mater.* 23, 4109–4111. doi: 10.1021/cm202076g

Shanmugam, R., and Lai, W. (2014). $Na_{2/3}Ni_{1/3}Ti_{2/3}O_2$: "bi-functional" electrode materials for Na-ion batteries. *Ecs Electrochem. Lett.* 3, A23–A25. doi: 10.1149/2.007404eel

Shen, K., and Wagemaker, M. (2014). $Na_2+xTi_6O_{13}$ as Potential negative electrode material for Na-ion batteries. *Inorg. Chem.* 53, 8250–8256. doi: 10.1021/ic5004269

Silbernagel, B. G., and Whittingham, M. S. (1976). An NMR study of the alkali metal intercalation phase $LixTiS_2$: relation to structure, thermodynamics, and ionicity. *J. Chem. Phys.* 64, 3670–3673. doi: 10.1063/1.432731

Slater, M. D., Kim, D., Lee, E., and Johnson, C. S. (2013). Sodium-ion batteries. *Adv. Funct. Mater.* 23, 947–958. doi: 10.1002/adfm.201200691

Song, W., Ji, X., Zhu, Y., Zhu, H., Li, F., Chen, J., et al. (2014). Aqueous sodium-ion battery using a $Na_3V_2(PO_4)_3$ electrode. *ChemElectroChem*. 1, 871–876. doi: 10.1002/celc.201300248

Su, D., Dou, S., and Wang, G. (2015). Anatase TiO_2: better anode material than amorphous and rutile phases of TiO_2 for Na-ion batteries. *Chem. Mater.* 27, 6022–6029. doi: 10.1021/acs.chemmater.5b02348

Sun, Q., Ren, Q-Q., Li, H., and Fu, Z-W. (2011). High capacity Sb_2O_4 thin film electrodes for rechargeable sodium battery. *Electrochem. Commun.* 13, 1462–1464. doi: 10.1016/j.elecom.2011.09.020

Sun, Y., Zhao, L., Pan, H., Lu, X., Gu, L., Hu, Y-S., et al. (2013). Direct atomic-scale confirmation of three-phase storage mechanism in $Li_4Ti_5O_{12}$ anodes for room-temperature sodium-ion batteries. *Nat. Commun.* 4:1870. doi: 10.1038/ncomms2878

Tao, H., Zhou, M., Wang, R., Wang, K., Cheng, S., and Jiang, K. (2018). TiS_2 as an advanced conversion electrode for sodium-ion batteries with ultra-high capacity and long-cycle life. *Adv. Sci.* 1801021. doi: 10.1002/advs.201801021

Trinh, N. D., Crosnier, O., Schougaard, S., and Brousse, T. (2012). Synthesis, characterizations and electrochemical studies of $Na_2Ti_6O_{13}$ for sodium ion batteries. *ECS Trans*. 35, 91–98. doi: 10.1149/1.3655691

Usui, H., Yoshioka, S., Wasada, K., Shimizu, M., and Sakaguchi, H. (2015). Nb-doped rutile TiO_2: a potential anode material for Na-ion battery. *ACS Appl. Mater. Interfaces* 7, 6567–6573. doi: 10.1021/am508670z

Wagemaker, M., Van Eck, E. R., Kentgens, A. P., and Mulder, F. M. (2008). Li-ion diffusion in the equilibrium nanomorphology of spinel $Li_{4+x}Ti_5O_{12}$. *J. Phys. Chem. B* 113, 224–230. doi: 10.1021/jp8073706

Wang, S., Wang, L., Zhu, Z., Hu, Z., Zhao, Q., and Chen, J. (2014). All organic sodium-ion batteries with $Na_4C_8H_2O_6$. *Angew. Chem. Int. Ed.* 53, 5892–5896. doi: 10.1002/anie.201400032

Wang, Y., Feng, Z., Laul, D., Zhu, W., Provencher, M., Trudeau, M. L., et al. (2018a). Ultra-low cost and highly stable hydrated $FePO_4$ anodes for aqueous sodium-ion battery. *J. Power Sour.* 374, 211–216. doi: 10.1016/j.jpowsour.2017.10.088

Wang, Y., Feng, Z., Zhu, W., Gariépy, V., Gagnon, C., Provencher, M., et al. (2018b). High capacity and high efficiency maple tree-biomass-derived hard carbon as an anode material for sodium-ion batteries. *Materials* 11:1294. doi: 10.3390/ma11081294

Wang, Y., Liu, J., Lee, B., Qiao, R., Yang, Z., Xu, S., et al. (2015a). Ti-substituted tunnel-type $Na0.44MnO_2$ oxide as a negative electrode for aqueous sodium-ion batteries. *Nat. Commun.* 6:6401. doi: 10.1038/ncomms7401

Wang, Y., Mu, L., Liu, J., Yang, Z., Yu, X., Gu, L., et al. (2015b). A novel high capacity positive electrode material with tunnel-type structure for aqueous sodium-ion batteries. *Adv. Energy Mater.* 5:1501005. doi: 10.1002/aenm.201501005

Wang, Y., Xiao, R., Hu, Y-S., Avdeev, M., and Chen, L. (2015c). P2-$Na_{0.6}[Cr_{0.6}Ti_{0.4}]O_2$ cation-disordered electrode for high-rate symmetric rechargeable sodium-ion batteries. *Nat. Commun.* 6:6954. doi: 10.1038/ncomms7954

Wang, Y. S., Yu, X. Q., Xu, S. Y., Bai, J. M., Xiao, R. J., Hu, Y. S., et al. (2013). A zero-strain layered metal oxide as the negative electrode for long-life sodium-ion batteries. *Nat. Commun.* 4:2365. doi: 10.1038/ncomms3365

Wei, Z., Ying, W., Zongling, H., and Jingze, L. (2014). Synthesis of $Na_2Ti_3O_7$@MWCNTs anode material by spray-drying method of sol-gel precursor for sodium-ion batteries. *Sci. Sin. Chim.* 44:1347. doi: 10.1360/N032014-00115

Wessells, C. D., Huggins, R. A., and Cui, Y. (2011a). Copper hexacyanoferrate battery electrodes with long cycle life and high power. *Nat. Commun.* 2:550. doi: 10.1038/ncomms1563

Wessells, C. D., Peddada, S. V., Huggins, R. A., and Cui, Y. (2011b). Nickel hexacyanoferrate nanoparticle electrodes for aqueous sodium and potassium ion batteries. *Nano Lett.* 11, 5421–5425. doi: 10.1021/nl203193q

Whitacre, J. F., Tevar, A., and Sharma, S. (2010). $Na_4Mn_9O_{18}$ as a positive electrode material for an aqueous electrolyte sodium-ion energy storage device. *Electrochem. Commun.* 12, 463–466. doi: 10.1016/j.elecom.2010.01.020

Wu, D., Li, X., Xu, B., Twu, N., Liu, L., and Ceder, G. (2015a). $NaTiO_2$: a layered anode material for sodium-ion batteries. *Energy Environ. Sci*. 8, 195–202. doi: 10.1039/C4EE03045A

Wu, L., Bresser, D., Buchholz, D., Giffin, G. A., Castro, C. R., Ochel, A., et al. (2015c). Unfolding the mechanism of sodium insertion in anatase TiO_2 nanoparticles. *Adv. Energy Mater.* 5:1401142. doi: 10.1002/aenm.201401142

Wu, L., Bresser, D., Buchholz, D., and Passerini, S. (2015b). Nanocrystalline TiO_2(B) as anode material for sodium-ion batteries. *J. Electrochem. Soc.* 162, A3052–A3058. doi: 10.1149/2.0091502jes

Wu, L., Hu, X., Qian, J., Pei, F., Wu, F., Mao, R., et al. (2014). Sb-C nanofibers with long cycle life as an anode material for high-performance sodium-ion batteries. *Energy Environ. Sci.* 7, 323–328. doi: 10.1039/C3EE42944J

Wu, W., Mohamed, A., and Whitacre, J. F. (2013). Microwave Synthesized $NaTi_2(PO_4)_3$ as an aqueous sodium-ion negative electrode. *J. Electrochem. Soc.* 160, A497–A504. doi: 10.1149/2.054303jes

Wu, X., Jin, S., Zhang, Z., Jiang, L., Mu, L., Hu, Y-S., et al. (2015d). Unraveling the storage mechanism in organic carbonyl electrodes for sodium-ion batteries. *Sci. Adv.* 1:e1500330. doi: 10.1126/sciadv.1500330

Xiao, L., Cao, Y., Xiao, J., Wang, W., Kovarik, L., Nie, Z., et al. (2012). High capacity, reversible alloying reactions in SnSb/C nanocomposites for Na-ion battery applications. *Chem. Commun.* 48, 3321–3323. doi: 10.1039/c2cc17129e

Xie, F., Zhang, L., Su, D., Jaroniec, M., and Qiao, S-Z. (2017). Na2Ti3O7@N-Doped carbon hollow spheres for sodium-ion batteries with excellent rate performance. *Adv. Mater.* 29:1700989. doi: 10.1002/adma.201700989

Xiong, H., Slater, M. D., Balasubramanian, M., Johnson, C. S., and Rajh, T. (2011). Amorphous TiO_2 nanotube anode for rechargeable sodium ion batteries. *J. Phys. Chem. Lett.* 2, 2560–2565. doi: 10.1021/jz2012066

Xu, J., Ma, C., Balasubramanian, M., and Meng, Y. S. (2014). Understanding $Na_2Ti_3O_7$ as an ultra-low voltage anode material for a Na-ion battery. *Chem. Commun.* 50, 12564–12567. doi: 10.1039/C4CC03973D

Yabuuchi, N., Yoshida, H., and Komaba, S. (2012). Crystal structures and electrode performance of alpha-$NaFeO_2$ for rechargeable sodium batteries. *Electrochemistry* 80, 716–719. doi: 10.5796/electrochemistry.80.716

Yang, Z., Zhang, J., Kintner-Meyer, M. C. W., Lu, X., Choi, D., Lemmon, J. P., et al. (2011). Electrochemical energy storage for green grid. *Chem. Rev.* 111, 3577–3613. doi: 10.1021/cr100290v

Yoshida, H., Yabuuchi, N., Kubota, K., Ikeuchi, I., Garsuch, A., Schulz-Dobrick, M., et al. (2014). P2-type $Na_{2/3}Ni_{1/3}Mn_{2/3-x}Ti_xO_2$ as a new positive electrode for higher energy Na-ion batteries. *Chem. Commun.* 50, 3677–3680. doi: 10.1039/C3CC49856E

Yu, H., Ren, Y., Xiao, D., Guo, S., Zhu, Y., Qian, Y., et al. (2014). An ultrastable anode for long-life room-temperature sodium-ion batteries. *Angew. Chem.* 126, 9109–9115. doi: 10.1002/ange.201404549

Zhang, B., Ghimbeu, C. M., Laberty, C., Vix-Guterl, C., and Tarascon, J. M. (2016). Correlation between microstructure and Na storage behavior in hard carbon. *Adv. Energy Mater.* 6:1501588. doi: 10.1002/aenm.201501588

Zhao, C., Avdeev, M., Chen, L., and Hu, Y-S. (2018a). An O3-type oxide with low sodium content as the phase-transition-free anode for sodium-ion batteries. *Angew. Chem. Int. Ed.* 57, 7056–7060. doi: 10.1002/anie.201801923

Zhao, C., Wang, Q., Lu, Y., Li, B., Chen, L., and Hu, Y-S. (2018b). High-temperature treatment induced carbon anode with ultrahigh Na storage capacity at low-voltage plateau. *Sci. Bull.* 63, 1125–1129. doi: 10.1016/j.scib.2018.07.018

Zhao, L., Pan, H-L., Hu, Y-S., Li, H., and Chen, L-Q. (2012a). Spinel lithium titanate ($Li_4Ti_5O_{12}$) as novel anode material for room-temperature sodium-ion battery. *Chinese Physics B* 21:28201. doi: 10.1088/1674-1056/21/2/028201

Zhao, L., Zhao, J., Hu, Y-S., Li, H., Zhou, Z., Armand, M., et al. (2012b).). Disodium terephthalate ($Na_2C_8H_4O_4$) as high performance anode material for low-cost room-temperature sodium-ion battery. *Adv. Energy Mater.* 2, 962–965. doi: 10.1002/aenm.201200166

Zhao, M., Huang, J., Guo, X., Chen, H., Zhao, H., Dong, L., et al. (2015). Preparation of $Na_2Ti_3O_7$/titanium peroxide composites and their adsorption property on cationic dyes. *J. Chem.* 2015:12. doi: 10.1155/2015/363405

Zheng, Y., Wang, Y., Lu, Y., Hu, Y-S., and Li, J. (2017). A high-performance sodium-ion battery enhanced by macadamia shell derived hard carbon anode. *Nano Energy* 39, 489–498. doi: 10.1016/j.nanoen.2017.07.018

Conflict of Interest Statement: YW, WZ, AG, CK, and KZ are employed by Hydro Quebec.